Int. J. Electrochem. Sci., 13 **(2018)** 7489 – 7504, doi: 10.20964/2018.08.64

International Journal of ELECTROCHEMICAL SCIENCE
www.electrochemsci.org

Effect of Bis-3-Sulfopropyl-Disulfide on the Characteristics of Trivalent Chromium Electrodeposition

Sol-Ji Song[1], *Sang Jin Ko*[1], *Jae-Ryung Lee*[2], *Jung-Gu Kim*[1,*]

[1] School of Advanced Materials Science and Engineering, Sungkyunkwan University, 300 Chunchun-Dong, Jangan-Gu, Suwon 440-746, Republic of Korea
[2] Research and Development Laboratory, POSCO, 6261, Donghaean-ro, Nam-gu, Pohang 37859, Republic of Korea
[*]E-mail: kimjg@skku.edu

Received: 3 April 2018 / *Accepted:* 7 June 2018 / *Published:* 5 July 2018

This study examined the effect of bis-3-sulfopropyl-disulfide (SPS) addition to chromium sulfate solution on the characteristics of trivalent chromium electrodeposition. To investigate the effect of SPS on current efficiency, electrodeposition was carried out on the Invar surface at a constant current over time. Electrochemical tests, surface and solution analyses, density functional theory calculation, and Vickers micro-hardness tests were conducted to identify the SPS mechanism and evaluate its properties. SPS addition improved the electrodeposition current efficiency more than two-fold by increasing the nucleation of the electrode and changing the Cr-complex in solution to increase the bonding length between trivalent chromium ions and water molecules. Also, the surface hardness and corrosion resistance of the electrodeposited specimen were improved in the SPS-containing solution.

Keywords: Trivalent chromium; Electrodeposition; Bis-3-sulfopropyl-disulfide; Current efficiency

1. INTRODUCTION

Hexavalent chromium coating has been widely used as a surface treatment in industrial applications due to its high wear resistance, corrosion resistance, and hardness [1,2]. However, because the hexavalent chromium electrodeposition solution is associated with environmental issues related to toxic steam, the industrial use of hexavalent chromium has been fully regulated [3-5]. Thus, trivalent chromium electrodeposition is considered a substitute for conventional hexavalent chromium electrodeposition because of its similar properties and eco-friendly qualities [6-8].

Many studies investigated the mechanism of trivalent chromium electrodeposition and have sought to increase the effectiveness of trivalent chromium baths. In aqueous solution, trivalent chromium ions (Cr^{3+}) combine with six water molecules to form thermodynamically stable esa-aquo

ion $[Cr(H_2O)_6]^{3+}$, hindering reduction of Cr^{3+} ions [9,10]. Therefore, the addition of a complexing agent such as acetic acid, formic acid, urea, or oxalic acid accelerates the reduction reaction of Cr^{3+} ions by making the $[Cr(H_2O)_6]^{3+}$ unstable due to the formation of a complex with Cr^{3+} ions, which are more thermodynamically stable than $[Cr(H_2O)_6]^{3+}$ [11-13]. In addition, there are many variables that affect trivalent chromium electrodeposition properties such as temperature, pH, current density, and electrodeposition time [14,15].

Cr^{3+} ions are reduced in two consecutive reduction steps [3,11,16]. The first step is conversion from Cr^{3+} species to Cr^{2+} species, and the second step is conversion from Cr^{2+} species to Cr(s):

$$Cr^{3+} + e^- \rightarrow Cr^{2+},\ E^0 = -0.41\ V_{SHE} \quad (1)$$

$$Cr^{2+} + 2e^- \rightarrow Cr(s),\ E^0 = -0.91\ V_{SHE} \quad (2)$$

where E^0 is the standard equilibrium potential of each equation at 25℃. In addition, during the reduction and electrodeposition of trivalent chromium, the hydrogen gas evolution reaction simultaneously occurs, which lowers the electrodeposition efficiency [17,18]. Also, the occurrence of hydrolysis and olation reactions inhibits reduction and electrodeposition of chromium ions [19-21].

For the enhancement of current efficiency, organic accelerator (or brightener) additives such as 3-mercaptopropionic acid (MPA), bis-3-sulfopropyl-disulfide (SPS) have been incorporated into copper electrodeposition. To promote electrodeposition, the organic additive must contain two functional groups: an adsorption group that chemically adsorbs onto the cathode, and a trapping group that serves to attract cations in solution by electrostatic attraction. In SPS, the sulfur-sulfur (S-S) bond acts as the adsorption group, and the sulfonate (SO_3^-) acts as the trapping group, playing critical roles in the acceleration mechanism [22-26].

Thus, the purpose of this study is to evaluate the effects of SPS on current efficiency and surface characteristics in trivalent chromium electrodeposition through electrochemical and mechanical testing, surface and solution analyses, and density functional theory with General Gradient Approximation/Perdew-Wang 91 (GGA/PW91) calculation.

2. EXPERIMENTAL

2.1. Chromium electrodeposition

Chromium electrodeposition was performed at a constant current density (2.0 A/dm^2) for varying times (30, 60, 90, and 120 sec). An iridium-coated titanium plate and 13-㎛-thick Invar (63.5 wt.% Fe, 36.5 wt.% Ni) were used for the anode and cathode, and the areas exposed to the solution were 10.0 cm × 23.0 cm and 7.5 cm × 16.5 cm, respectively. The distance between the anode and cathode was fixed at 2.05 cm. The cathode was degreased with ethanol and dried before the electrodeposition experiment. The chromium electrodeposition experiments were conducted at least twice for each solution and time condition.

The sulfate trivalent chromium electrodeposition solution contains: 75 g/L $Cr_2(SO_4)_3$ + H_2SO_4 as a source of Cr^{3+}, 320 g/L H_3BO_3 + KCl as a buffering and conducting agent, 15 ml/L polyethylene glycol to retard the hydrogen evolution reaction rate, and 30 g/L complexing agent + surfactant. To confirm the effect of the additive, 90 mg/L of additive SPS in solution was added. During electrodeposition, the solution was maintained at 45℃, and agitated with a pump to minimize the concentration polarization. The pH of the solution was maintained between 3.0 and 3.5 with 20 wt.% NaOH.

The thickness of electrodeposited chromium was measured by X-ray fluorescence (XRF, EDX-8000, Shimadzu) and the efficiency of electrodeposition was calculated from the measured thickness value. The average values of chromium thickness were calculated for each solution from six independent measurements.

2.2. Electrochemical tests

Electrochemical tests consisted of cyclic voltammetry (CV) and electrochemical impedance spectroscopy (EIS), which were conducted on the three-electrode system using the multi-potentiostat / galvanostat VSP-300. A saturated calomel electrode (SCE) and iridium-coated titanium plate were used as the reference electrode and the counter electrode, respectively. In CV measurement, the 13-㎛-thick Invar was used, while the Invar electrodeposited at 2.0 A/dm^2 for 120 sec was used as the working electrode in EIS measurement.

The CV was measured to obtain the reaction information for the working electrode surface of 13-㎛-thick Invar [27,28]. The CV experiment was performed at a potential range from -0.4 V_{SCE} to -1.6 V_{SCE} at a scan rate of 50 mV/s. The composition of the solution used in the CV was the same as that of the sulfate trivalent chromium electrodeposition solution with and without SPS at 45℃.

EIS tests were carried out to calculate the corrosion rate and to observe the change in the electrodeposited chromium layer caused by SPS addition. EIS measurement was conducted in 3.5 wt.% NaCl solution with an exposed area of 0.25 cm^2 at room temperature. Before EIS measurements, a stable open-circuit potential (OCP) was established within 12 hours. After the specimens reached a stable OCP, EIS measurement was performed at a sinusoidal amplitude of 10 mV with frequencies ranging from 100 kHz to 1 mHz. Using the Zsimpwin software, impedance plots were interpreted on the basis of an equivalent circuit according to a suitable fitting procedure.

2.3. Surface and solution analyses

To determine the role of SPS in trivalent chromium electrodeposition, the surface morphology of the chromium deposit was investigated via scanning electron microscopy (SEM, JSM 7000F, JEOL) and atomic force microscopy (AFM, XE7, Park systems). In AFM measurement, contact mode with force modulation-type cantilever was used and typical applied forces are about 30 nN at a scan rate of 0.5 Hz. X-ray diffraction (XRD, D8 ADVANCE, Bruker) analysis was performed to confirm the

chromium phase using a monochromatic Cu Kα energy source with a scan rate of 3 °/min from 10° to 100°.

UV-VIS spectrometer (UV-VIS, Cary 5000, Varlan) measurement of the electrodeposition solution was conducted in the presence or absence of SPS to observe changes in Cr-complexes due to interaction with SPS. UV-VIS absorption was measured from 750 to 300 nm wavelengths.

2.4. Geometric structure simulation

The equilibrium geometric structures of the initial and transformed state ions were calculated using density functional theory with GGA/PW91 simulation, which is widely used to optimize the geometric structure of compounds [13,29,30]. The geometric structure was described using B31YP with a base set 6-31++G(d,p) using the GAUSSIAN-09 program.

2.5. Hardness

Vickers micro-hardness (HV, Mitutoyo MVK-H2) measurements were conducted on the chromium electrodeposited specimens at a load of 200 gf for 10 s. The hardness test was carried out at the center of the specimens. The average hardness values were calculated for each specimen from more than 10 independent measurements.

3. RESULTS AND DISCUSSION

3.1. Effect of SPS on the current efficiency of chromium electrodeposition

Figure 1 represents the Cr-thickness and current efficiency of chromium electrodeposition with various electrodeposition times at 2.0 A/dm^2. In Fig. 1, blank means the solution of sulfate trivalent chromium and blank + SPS 90 ppm means the solution of sulfate trivalent chromium with the addition of SPS 90 ppm. The current efficiency of chromium electrodeposition was calculated using the following equation with Faraday's law [31,32]:

$$Current efficiency\,(\eta\%) = \frac{T(cm)\times A(cm^2)\times S}{I(A)\times t(sec)\times E.C.E(g/C)}\times 100 \quad (3)$$

where T is the electrodeposited chromium thickness measured by XRF, A is the area of the cathode (123.75 cm^2), S is the specific density of chromium (7.19 g/cm^3), I is the applied current for electrodeposition (2.0 A/dm^2), t is the time of current application, and $E.C.E$ is the electrochemical equivalent of trivalent chromium (1.79E^{-4} g/C). As the electrodeposition time increased, the Cr-thicknesses also increased. Notably, the current efficiency increased 19.06% with the addition of SPS

to the electrodeposition solution. This means that SPS accelerates the reduction and electrodeposition of chromium ions by changing the reaction mechanism.

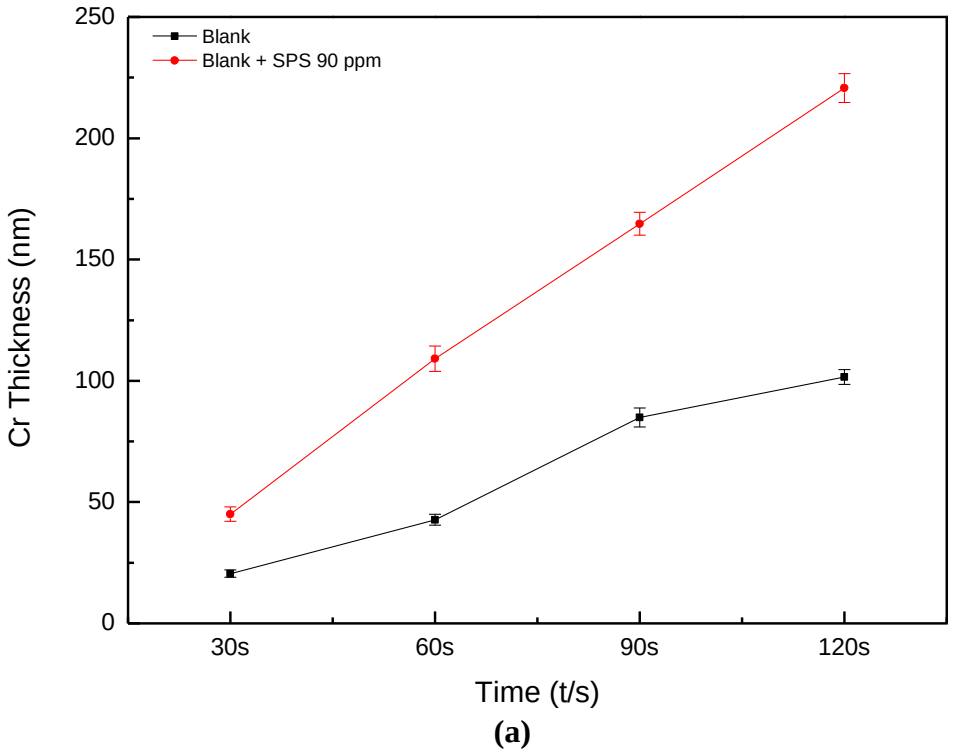

(a)

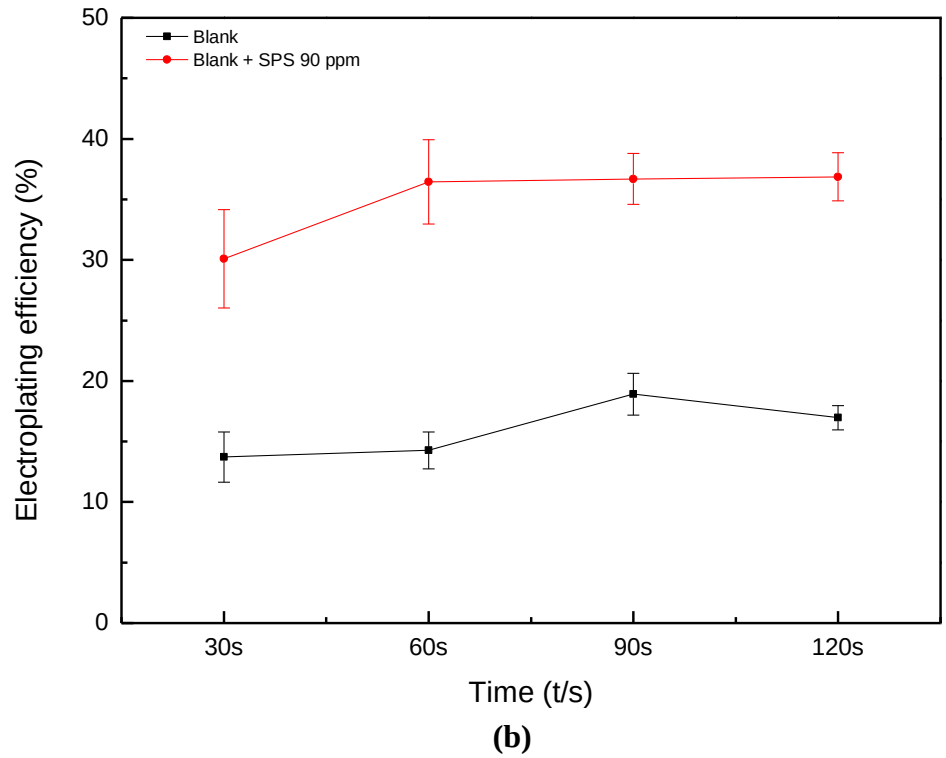

(b)

Figure 1. Results of chromium electrodeposition at blank and blank + SPS 90 ppm solutions (a) chromium thickness and (b) current efficiency at 2.0 A/dm^2 with time.

3.2. Cyclic voltammetry

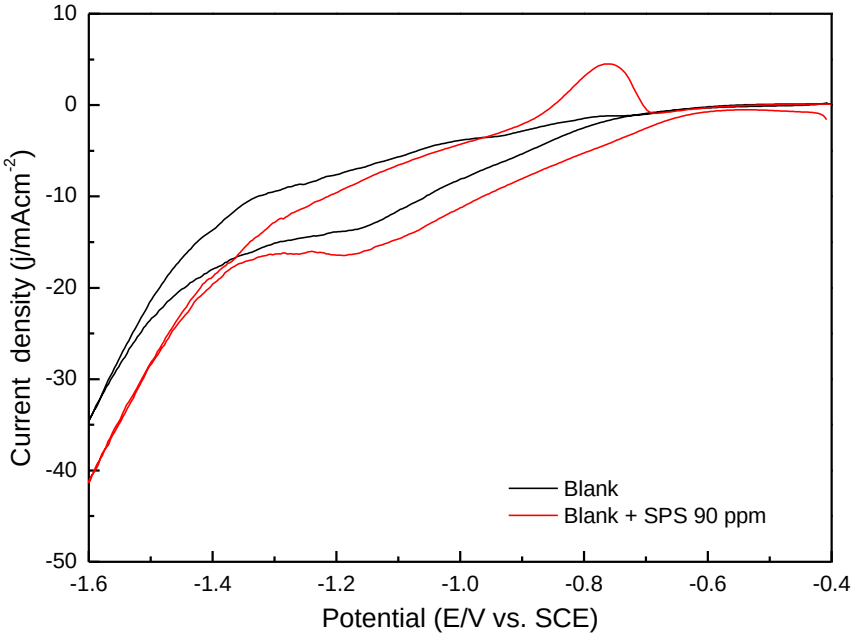

Figure 2. Cyclic voltammograms of blank and blank + SPS 90 ppm solutions on Invar at 50 mV/s.

The CV results of the electrochemical reduction reaction with and without SPS are shown in Fig. 2. Depending on the presence or absence of SPS, major differences are indicated by initial potential and current density. The change in the initial potential by SPS addition is related to the adsorption of SPS to the solution and the electrode interface [33]. From an atomistic point of view, electrodeposition is carried out by a direct mechanism or a terrace site ion mechanism. However, the adsorbed additive influenced both mechanisms by changing the concentration of growth sites on the surface, the diffusion coefficient, and the activation energy of adion surface diffusion [31,34]. In addition, the adsorbed additive acted on the nucleation and growth mechanism of reduced and electrodeposited metal ions. Therefore, the adsorption of SPS on the surface affected nucleation and growth, thereby accelerating the reduction and electrodeposition of trivalent chromium ions in solution. Also, the SPS-containing solution showed a higher current density as an absolute value than the solution without SPS. Having a higher current density at the same potential implies an accelerated electrodeposition rate and thus increased current efficiency. Therefore, these results indicate that SPS interacts with the trivalent chromium complexes in solution [35,36].

3.3. Surface and solution analyses

Figure 3 shows the SEM results of the top surface and 45° tilted surface of the electrodeposited specimens at 2.0 A/dm^2 for 120 s, with and without SPS. As shown in the top surface morphology, the surface contains a number of spheroids, reflecting the increased number of nucleation sites from the

addition of SPS. Also, the 45° tilted surface demonstrates that SPS addition reduced defects compared with the specimen without SPS. AFM measurement can demonstrate the surface roughness directly. Figures 4(a) and (b) represent the AFM results of the specimens without and with SPS, respectively. As shown in Fig. 4, the surface roughness of the specimens, i.e., average surface roughness (R_a), root mean square roughness (R_q), and mean roughness depth (R_z) of whole AFM images, is decreased sharply by addition of SPS. Therefore, it can be seen that the addition of SPS increases the nucleation and decreases the surface roughness.

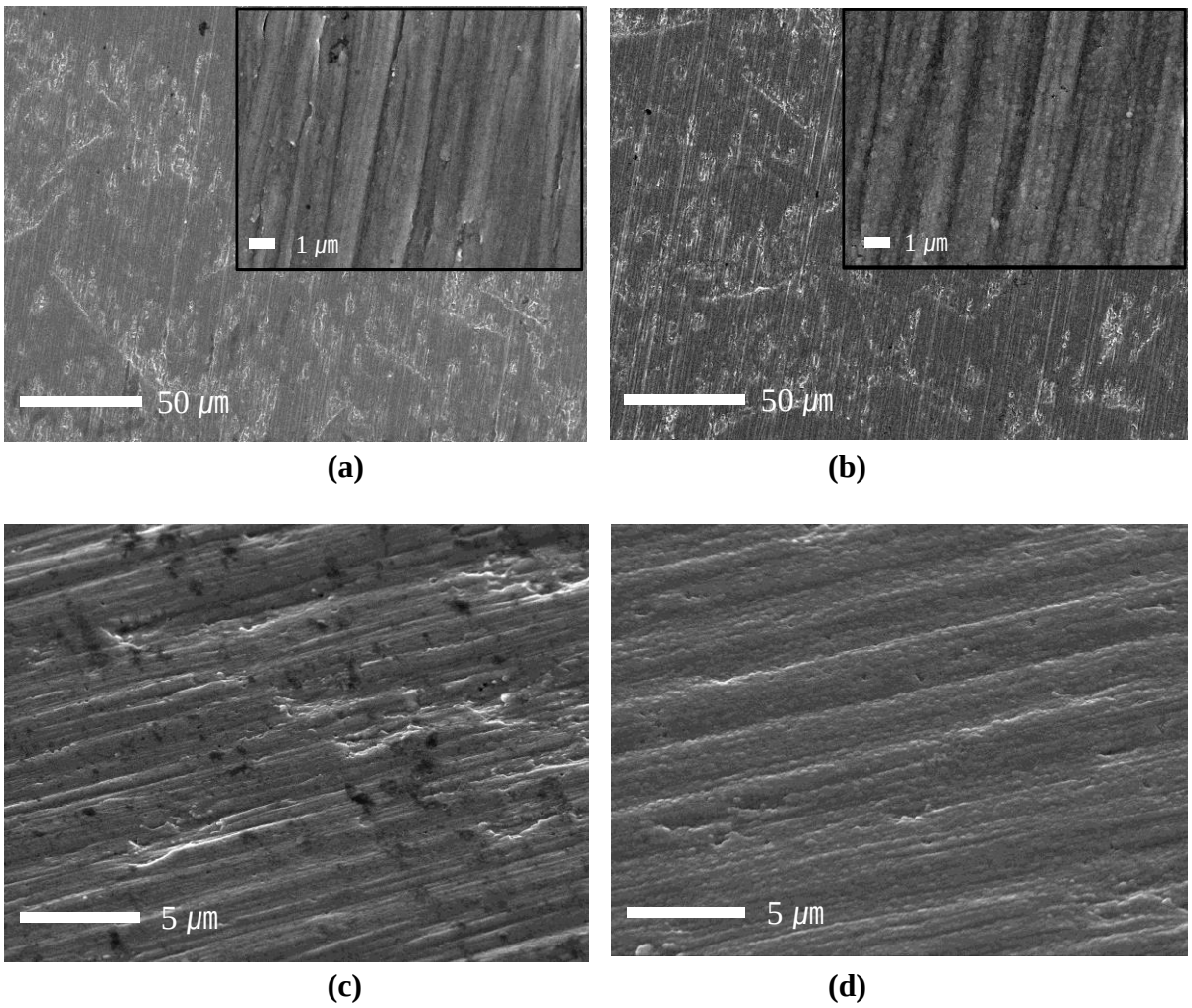

Figure 3. SEM images of electrodeposited specimens on (a) top surface in blank solution, (b) top surface in blank + SPS 90 ppm solution, (c) 45° tilted surface in blank solution, and (d) 45° tilted surface in blank + SPS 90 ppm solution.

The XRD patterns of the electrodeposited surfaces in chromium solution with and without SPS are shown in Fig. 5. The main peak of the electrodeposited specimen was the chromium (110) plane, and the other peak was chromium carbide with a chemical composition of $Cr_{23}C_6$. In trivalent chromium electrodeposition, chromium carbide (Cr-C) deposits can be obtained because the addition of the complexing agent prevents olation reactions [37,38].

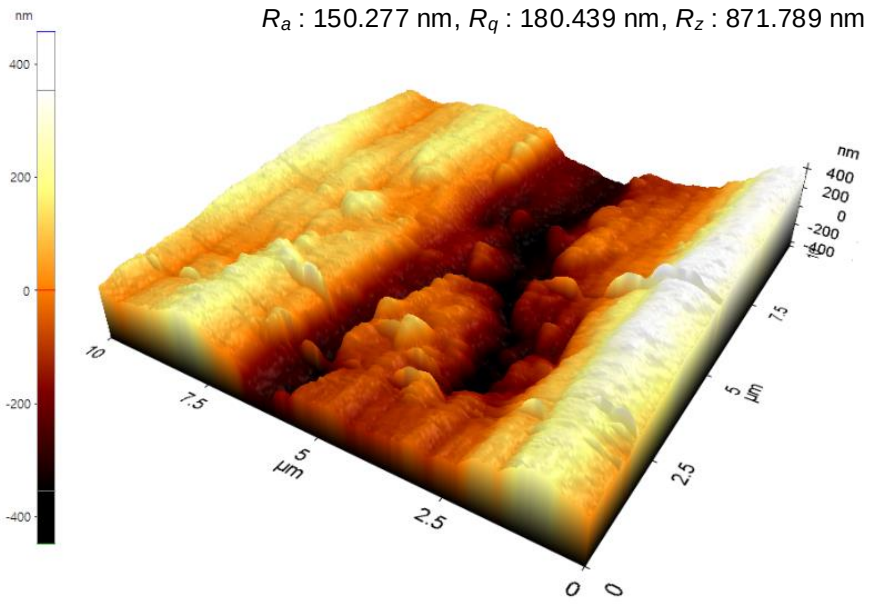

(a)

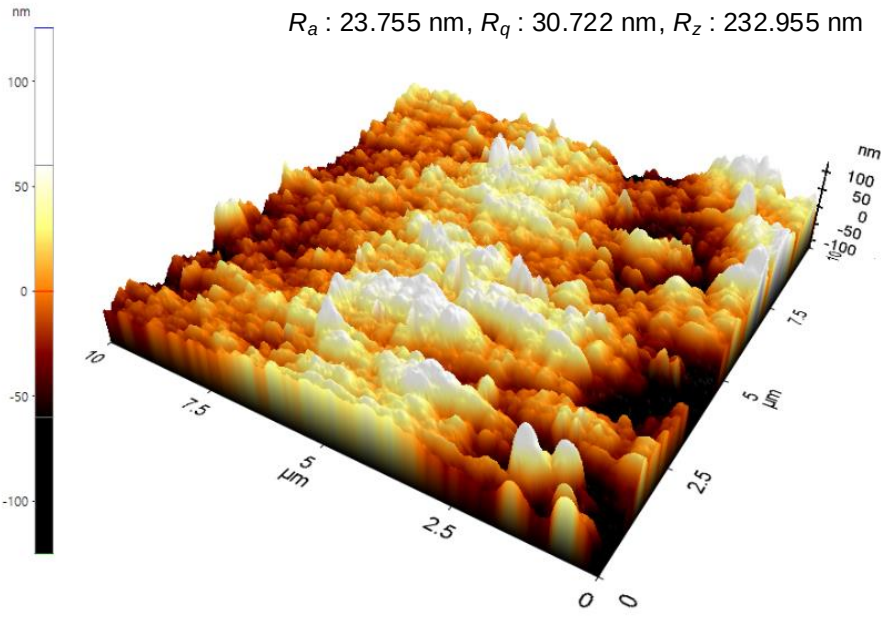

(b)

Figure 4. AFM images representing the change in surface roughness of chromium electrodeposit in blank and blank + SPS 90 ppm solutions.

The precipitation of Cr-C is related to the hardness of the specimen [37-40]. To estimate chromium grain size, the XRD results were interpreted with the *Scherrer's* equation [26,41]:

$$d = \frac{k\lambda}{\beta \cos\theta} \qquad (4)$$

where d is the grain size, k is the Scherrer constant, λ is the X-ray wavelength on Cu Kα, β is the full width at half maximum (FWHM), and θ is the Bragg diffraction angle. The grain size of the chromium deposit was 4.89 nm and 5.11 nm with and without SPS in solution, respectively. The increase of nucleation in the electro-crystallization process suppresses grain growth and causes a decrease in grain size. Therefore, the decreased grain size with the addition of SPS in solution indicates increased nucleation of the electrode surface [42].

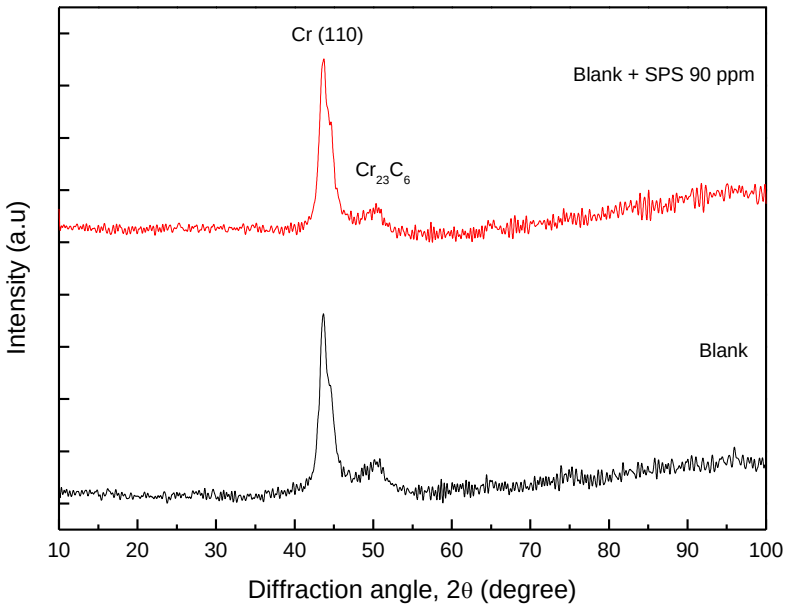

Figure 5. XRD spectra of chromium electrodeposit in blank and blank + SPS 90 ppm solutions.

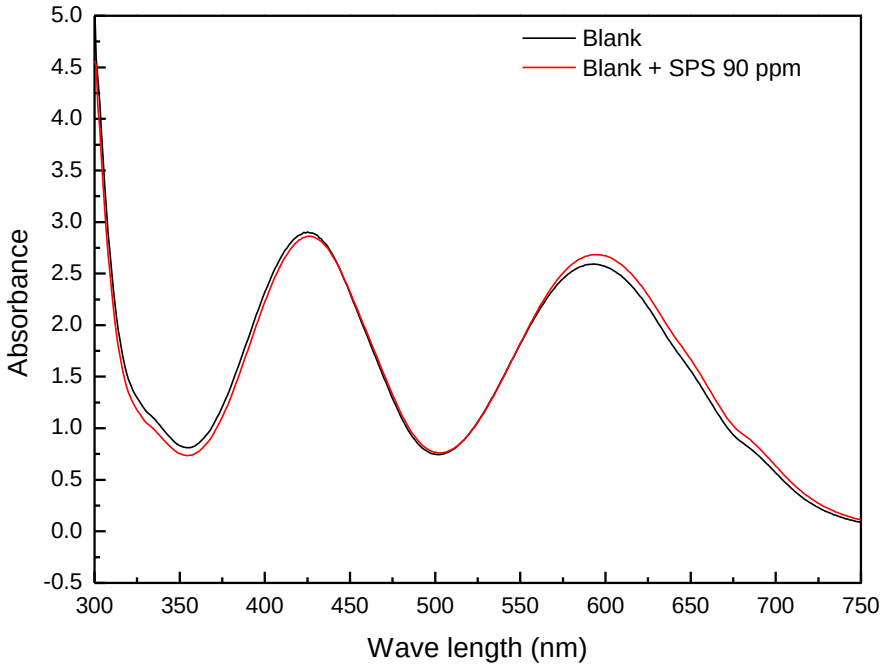

Figure 6. UV-VIS absorption spectra of blank and blank + SPS 90 ppm solutions.

UV-VIS measurement results are presented in Fig. 6. The addition of SPS increased absorbance as a whole, and the wavelength is shifted by SPS addition (SPS addition changed the wavelength from 425 nm to 427 nm and from 591 nm to 596 nm). Yao et al. [43] demonstrated that the increase in peak wavelength is due to the change in the form of trivalent chromium ions in the solution from $[Cr(H_2O)_6]^{3+}$ to $[Cr(H_2O)_5(OH)]^{2+}$. In that study, the concentration of $[Cr(H_2O)_5(OH)]^{2+}$ was relatively higher when SPS was added to the solution. Also, Song et al. [44] mentioned that the $[Cr(H_2O)_5(OH)]^{2+}$ complex in solution acts as an active component in the electrochemical reduction reaction of trivalent chromium electrodeposition processes. Therefore, in this study, SPS addition accelerates the reduction of trivalent chromium electrodeposition by forming more $[Cr(H_2O)_5(OH)]^{2+}$, which accelerates electrodeposition.

3.4. Structural analysis with density functional theory simulation

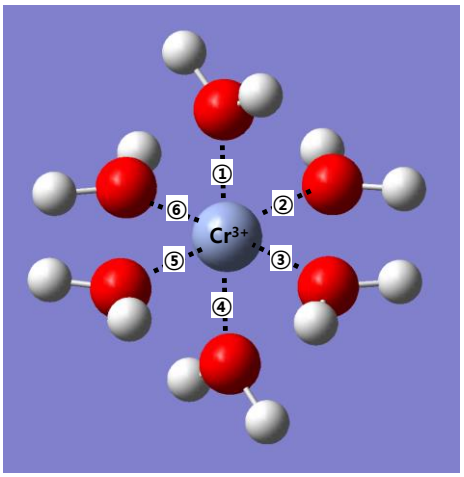

(a)

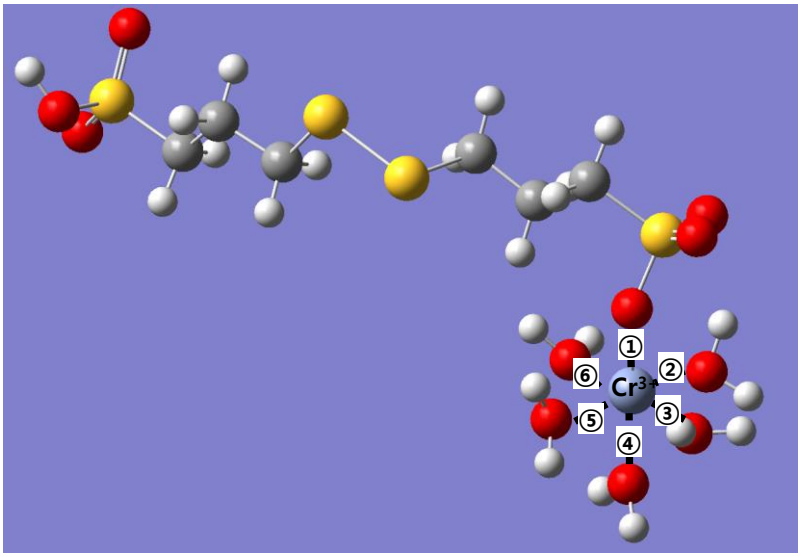

(b)

Figure 7. Equilibrium geometric structures of (a) without additive; $[Cr(H_2O)_6]^{3+}$, and (b) with additive; $[Cr(H_2O)_5(C_6H_{13}O_6S_4)]^{2+}$.

Table 1. Bonding length of the numerically marked on each Cr-complex (Å).

Cr-complex	①	②	③	④	⑤	⑥
$[Cr(H_2O)_6]^{3+}$	1.959	1.984	1.958	1.961	1.985	1.955
$[Cr(H_2O)_5(C_6H_{13}O_6S_4)]^{2+}$	1.865	2.002	2.009	2.059	2.012	2.013

As the aqua complex formed by the metal ions in the electrodeposition affects the reduction and electrodeposition reaction, it is necessary to study its geometric structure. Thus, to confirm the geometric structural change of the chromium-complex, a density functional theory simulation was conducted and is presented in Fig. 7. Trivalent chromium ion is associated with six water molecules, which numbered for six bond lengths between each water molecule and trivalent chromium ion. Table 1 lists the change in bonding length between trivalent chromium ions and water molecules with and without additives. The calculated average distance between trivalent chromium ions and water molecules before adding SPS was about 1.97 Å, but the maximum distance after adding SPS was 2.06 Å. In the SPS-containing solution, the force between trivalent chromium ions and the SPS was stronger than that of water molecules. The distance between SPS and trivalent chromium ions decreased, while the distance between trivalent chromium ions and water molecules at opposite positions increased significantly and other distance also increased slightly. Zeng et al. mentioned that the increase in bonding length facilitates the reduction reaction of chromium ions on the cathode [13]. In particular, if the distance between metal ions and water molecules is larger than 2.04 Å, it is easily electrodeposited, but if it is smaller than 2.04 Å, it is difficult to electrodeposit. Therefore, the addition of SPS increased the distance between trivalent chromium ions and water molecules by more than 2.04 Å, which facilitated electrodeposition. This is thought to have caused the observed increase in electrodeposition efficiency. The SPS with the formula $C_6H_{14}O_6S_4$ loses one hydrogen ion of the hydroxyl group (-OH) when it is bonded with trivalent chromium ion and replace position with one water molecule surrounding trivalent chromium ion. Therefore, the equilibrium geometric structure is changed to the $[Cr(H_2O)_5(C_6H_{13}O_6S_4)]^{2+}$ complex.

3.5. Characteristics of mechanical and corrosion resistance

The average hardness value and standard deviation of the electrodeposited specimen with and without SPS at 2.0 A/dm^2 for 120s are indicated in Fig. 8. The hardness of the specimen electrodeposited in the SPS-containing solution increased about 50 HV. The hardness of chromium deposits is highly dependent on grain size, residual stress, and inclusion content such as metallic and nonmetallic phases. In the XRD data, the $Cr_{23}C_6$ peak had a higher intensity when SPS was added, which indicates the formation of more $Cr_{23}C_6$; thus, the electrodeposited specimen exhibited a greater

hardness in the solution containing SPS. This increase in surface hardness with SPS addition is due to grain refinement, increased formation of chromium carbide, and greater chromium thickness.

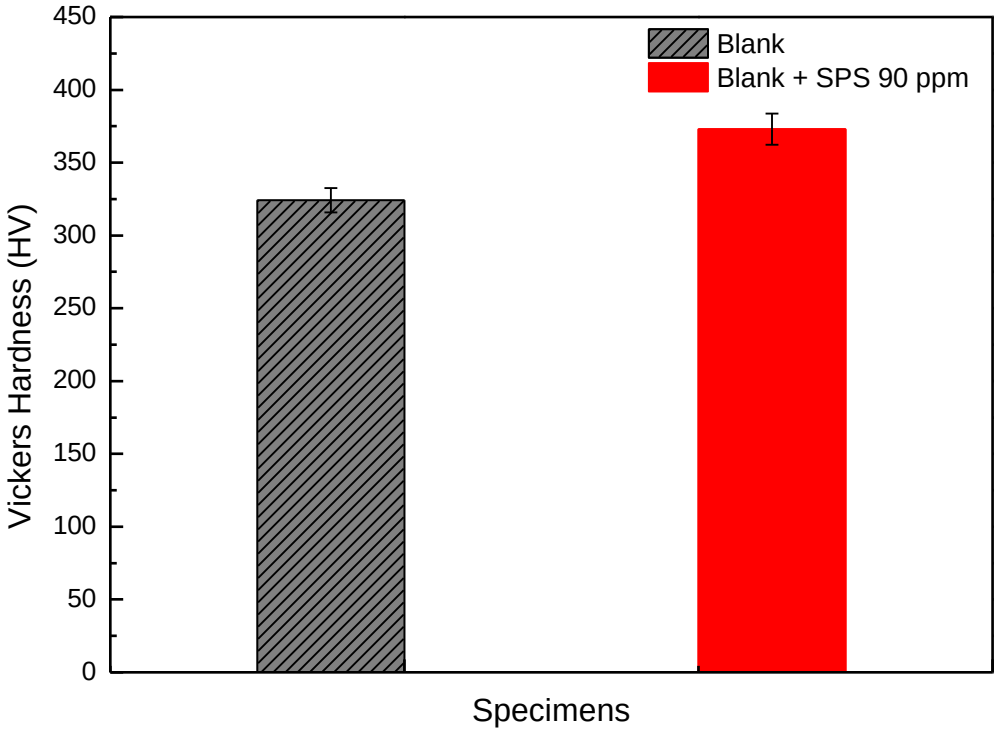

Figure 8. Vickers hardness of electrodeposited specimen surface in blank and blank + SPS 90 ppm solutions.

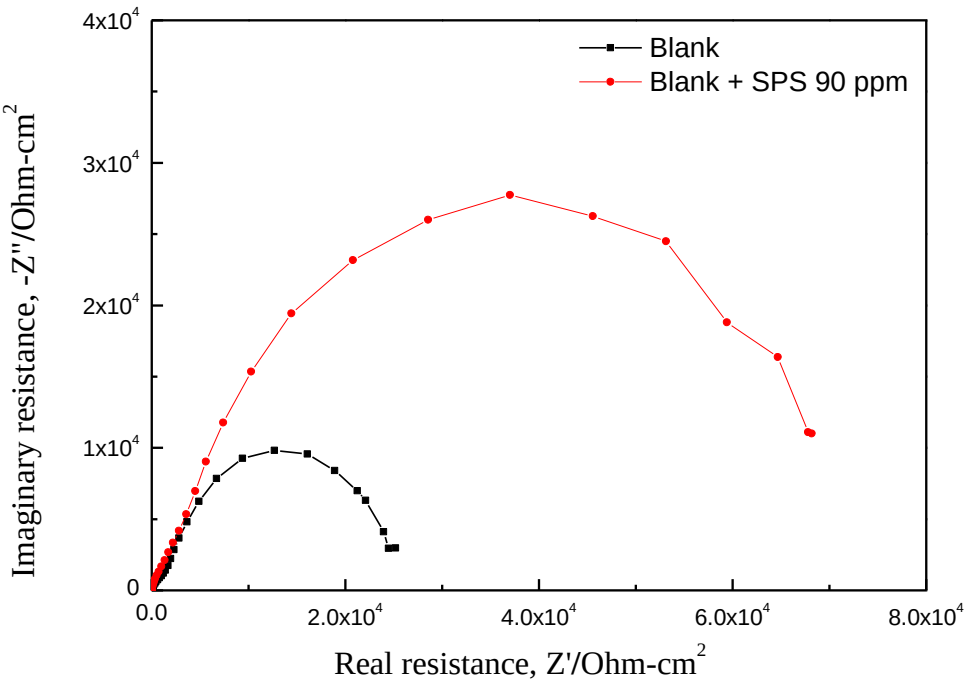

Figure 9. Nyquist plots in 3.5 wt.% NaCl at 25°C as a function of SPS in solution during electrodeposition process.

Figure 9 shows the Nyquist plots obtained for the electrodeposited specimen in 3.5 wt.% NaCl solution as a function of the presence of SPS in solution during the electrodeposition process. The EIS results demonstrated that the corrosion resistance of the electrodeposited specimen increased in the SPS-containing solution. Figure 10 presents an equivalent circuit used for fitting the EIS results. The Nyquist plots show the two-time constant behavior due to the electrodeposited chromium on the Invar surface. The equivalent circuit consists of the following elements: the solution resistance (R_s), electrodeposited chromium resistance (R_{Cr}), chromium capacitance (C_{Cr} (CPE1)), charge transfer resistance (R_{ct}), and double-layer capacitance generated by the electric double layer capacitance between the solution and the specimen interface (C_{dl} (CPE2)). In the circuit, the constant phase element (CPE) was used instead of the pure capacitance for a more accurate fit [45]. The impedance of the CPE takes the form of :

$$Z_{CPE} = \frac{1}{Y_0(j\omega)^n} \qquad (5)$$

where Y_0 is the magnitude of CPE, ω is the sine wave modulation angular frequency, j is an imaginary number, and n is the depression parameter ($0 \leq n \leq 1$) caused by frequency dispersion due to surface characteristics such as roughness and non-homogeneity [45-48]. The CPE expresses the ideal capacitor when n = 1.

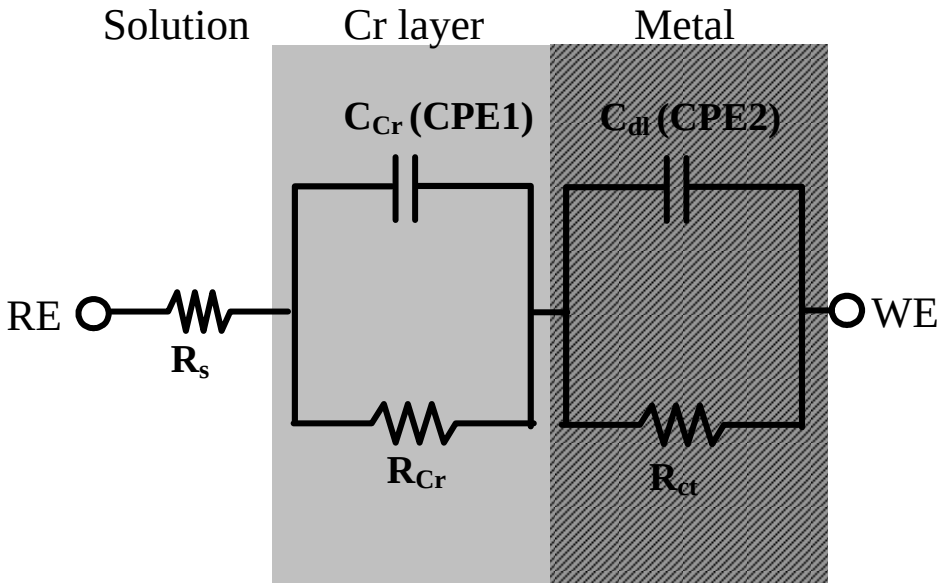

Figure 10. Equivalent circuit for fitting the EIS result for electrodeposited specimen in 3.5 wt.% NaCl at 25°C.

Table 2 summarizes the impedance parameters for specimens that were electrodeposited in the solution with and without SPS. The increase in R_{Cr} and R_{ct} in the SPS-containing solution indicates that the resistance of the chromium layer to corrosion increased and the charge transfer reaction decreased, respectively.

The capacitance can be expressed by the following equation [49,50]:

$$C = \frac{\varepsilon \varepsilon_0 A}{d} \quad (6)$$

where ε is the dielectric constant of the chromium layer or Helmholtz electrical double layer, ε_0 is the vacuum permittivity, d is the thickness of the chromium layer or Helmholtz electrical double layer, and A is the effective surface area of the electrode.

Table 2. EIS parameters for trivalent chromium electrodeposit in blank and blank + SPS 90 ppm solutions in 3.5 wt.% NaCl at 25℃.

Specimen	R_s (Ω-cm^2)	CPE1		R_{Cr} (Ω-cm^2)	CPE2		R_{ct} (Ω-cm^2)
		C_{Cr} (F/cm^2)	n (0-1)		C_{dl} (F/cm^2)	n (0-1)	
Blank	8.833	8.90×10^{-5}	0.8463	1208	3.16×10^{-4}	0.8386	2.48×10^{4}
SPS addition	3.360	8.38×10^{-5}	0.8953	1511	1.28×10^{-4}	0.8143	7.25×10^{4}

The decrease in C_{Cr} and increase in n in the SPS-containing solution indicate that the thickness of the electrodeposited chromium increased (Fig. 1), and the chromium layer is more stable. Also, these changes in the chromium layer affected the increase of R_{ct} through the inhibition of water molecule adsorption on the Invar surface.

4. CONCLUSIONS

The effect of bis-3-sulfopropyl-disulfide (SPS) on the characteristics of trivalent chromium electrodeposition was investigated using electrodeposition, electrochemical tests, surface and solution analysis, density functional theory with GGA/PW91 calculation, and Vickers micro-hardness. The following conclusions were reached:

(1) Through electrodeposition with various electrodeposition times (30, 60, 90, and 120 s) at 2.0 A/dm^2, electrodeposition current efficiency increased 19.06% on average with SPS addition.

(2) The CV test showed an initial potential change due to the adsorption of SPS at the solution and electrode interface. The adsorbed SPS increased the nucleation sites on the surface, increasing the spherical shape in SEM, and decreasing the grain size and surface roughness in XRD and AFM, respectively.

(3) UV-VIS measurements demonstrated that SPS addition increased the $[Cr(H_2O)_5(OH)]^{2+}$

complex in solution, which acts as an active component in the electrochemical reduction reaction. Also, the $[Cr(H_2O)_5(C_6H_{13}O_6S_4)]^{2+}$ complex, through the density functional theory simulation, increased the bonding length between trivalent chromium ions and water molecules to facilitate the electrodeposition reaction of chromium ions.

(4) The SEM results demonstrated that the electrodeposited specimen with SPS decreased defects. The addition of SPS also improved the corrosion resistance. Furthermore, surface hardness was increased due to increase in grain refinement, chromium carbide ($Cr_{23}C_6$) formation and chromium thickness.

References

1. P. de Lima-Neto, G.P. da Silva and A.N. Correia, *Electrochim. Acta*, 51 (2006) 4928.
2. X. He, C. Li, Y. Jiang, Q. Zhu, W. Wang, C. Zhang and L. Wu, *J. Electrochem. Soc.*, 162 (2015) D435.
3. U.P. Kumar and C.J. Kennady, *Int. J. Thin. Fil. Sci. Tec.*, 4 (2015) 147.
4. F.I. Danilov, V.S. Protsenko, V.O. Gordiienko, S.C. Kwon, J.Y. Lee and M. Kim, *Appl. Surf. Sci.*, 257 (2011) 8048.
5. E.S.C. Ferreira, C.M. Pereira and A.F. Silva, *J. Electroanal. Chem.*, 707 (2013) 52.
6. V.S. Protsenko, V.O. Gordiienko and F.I. Danilov, *Electrochem. Commun.*, 17 (2012) 85.
7. Z. Zeng, L. Wang, A. Liang and J. Zhang, *Electrochim. Acta*, 52 (2006) 1366.
8. Y. Choi, *Met. Mater. Int.*, 16 (2010) 755.
9. Z. Zeng, Y. Sun and J. Zhang, *Electrochem. Commun.*, 11 (2009) 331.
10. S. Survilienė, O. Nivinskienė, A. Češunienė and A. Selskis, *J. Appl. Electrochem.*, 36 (2006) 649
11. V. Protsenko and F. Danilov, *Electrochim. Acta*, 54 (2009) 5666.
12. C.E. Lu, J.L. Lee, H.H. Sheu, K.H. Hou, C.C. Tseng and M.D. Ger, *Int. J. Electrochem. Sci.*, 10 (2015) 5405.
13. Z. Zeng, Y. Zhang, W. Zhao and J. Zhang, *Surf. Coat. Technol.*, 205 (2011) 4771.
14. Protsenko, V.O. Gordiienko, F.I. Danilov and S.C. Kwon, *Met. Finish.*, 109 (2011) 33.
15. V.S. Protsenko, F.I. Danilov, V.O. Gordiienko, S.C. Kwon, M. Kim, and J.Y. Lee, *Thin Solid Films*, 520 (2011) 380.
16. F.I. Danilov, V.S. Protsenko, V.O. Gordiienko, A.S. Baskevich and V.V. Artemchuk, *Prot. Met. Phys. Chem.*, 49 (2013) 299.
17. J. Szynkarczuk, I. Drela and J. Kubicki, *Electrochim. Acta*, 34 (1989) 399.
18. R. Giovanardi and G. Orlando, *Surf. Coat. Technol.*, 205 (2011) 3947.
19. A. Baral and R. Engelken, *J. Electrochem. Soc.*, 152 (2005) C504.
20. C. Kasper, *Bur. Standards. J. of Research 9*, (1932) 353.
21. D. Rai, B.M. Sass and D.A. Moore, *Inorg. Chem.*, 26 (1987) 345.
22. K. Kondo, R.N. Akolkar, D.P. Barkey and M. Yokoi, *Copper Electrodeposition for Nanofabrication of Electronic Devices*, Springer, (2014) New York.
23. Y.D. Chiu, and W.P. Dow, *J. Electrochem. Soc.*, 160 (2012) D3021.
24. T.M.T. Huynh, F. Weiss, N.T.M. Hai, W. Reckien, T. Bredow, A. Fluegel, M. Arnold, D. Mayer, H. Keller and P. Broekmann, E*lectrochim. Acta*, 89 (2013) 537.
25. M. Tan, C. Guymon, D.R. Wheeler and J.N. Harb, *J. Electrochem. Soc.*, 154 (2007) D78.
26. S.J. Song, S.R. Choi, J.G. Kim and H.G. Kim, *Int. J. Electrochem. Sci.*, 11 (2016) 10067.
27. S. Eugénio, C.M. Rangel, R. Vilar and S. Quaresma, *Electrochim. Acta*, 56 (2011) 10347.
28. X. He, C. Li, Q. Zhu, B. Hou, Y. Jiang and L. Wu, *RSC Adv.*, 4 (2014) 64174.
29. P.L. Silvestrelli and A. Ambrosetti, *Phys. Rev. B: Condens. Matter*, 87 (2013) 075401-1.

30. K.P. Ong, K. Bai, P. Blaha and P. Wu, *Chem. Mater.*, 19 (2007) 634.
31. M. Schlesinger and M. Paunovic, *Modern Electroplating*, John Wiley & Sons, (2011) New Jersey.
32. Y.D. Gamburg and G. Zangari, *Theory and Practice of Metal Electrodeposition*, Springer Science & Business Media, (2011) New York.
33. J.Y. Lee, M. Kim and S.C. Kwon, *T. Nonferr. Metal. Soc.*, 19 (2009) 819.
34. M. Paunovic and M. Schlesinger, *Fundamentals of Electrochemical Deposition*, John Wiley & Sons, (2006) New Jersey.
35. P. Broekmann, A. Fluegel, C. Emnet, M. Arnold, C. Roeger-Goepfert, A. Wagner, N.T.M. Hai and D. Mayera, *Electrochim. Acta*, 56 (2011) 4724.
36. A. Chrzanowska and R. Mroczka, *Electrochim. Acta*, 78 (2012) 316.
37. S. Ghaziof, K. Raeissi and M.A. Golozar, *Surf. Coat. Technol.*, 205 (2010) 2174.
38. S. Ghaziof, M.A. Golozar and K. Raeissi, *J. Alloys Compd.*, 496 (2010) 164.
39. C.A. Huang, Y.W. Liu and C.H. Chuang, *Thin Solid Films* 517 (2009) 4902.
40. C.A. Huang, Y.W. Liu, C. Yu and C.C. Yang, *Surf. Coat. Technol.*, 205 (2011) 3461.
41. E.J. Mittemeijer and P. Scardi, *Diffraction Analysis of the Microstructure of Materials*, Springer Science & Business Media, (2013) New York.
42. R. Manu and S. Jayakrishnan, *Bull. Mater. Sci.*, 34 (2011) 347.
43. Y. Yao, Q. Wei, M. Sun, Y. Chen and X. Ren, *RSC Adv.*, 3 (2013) 13131.
44. Y.B. Song and D.T. Chin, *Electrochim. Acta*, 20 (2002) 349.
45. J.R. Macdonald and W.B. Johanson, *Theory in Impedance Spectroscopy*, John Wiley & Sons, (1987) New York.
46. F. Bentissa, M. Lebrini, H. Vezin, F. Chai, M. Traisnel and M. Lagrene, *Corros. Sci.*, 51 (2009) 2165.
47. Y.S. Kim and J.G. Kim, *Mater. Trans.*, 58 (2017) 76.
48. F. Mansfeld, M.W. Kending, and T. Tsai, *Corrosion*, 38 (1982) 570.
49. C. Bataillon and S. Brunet, *Electrochim. Acta*, 39 (1994) 455.
50. H. H. Hassan, *Electrochim. Acta*, 51 (2006) 5966.